

## SLURRY-BASED LASER SINTERING OF ALUMINA CERAMICS

Sebastian Meyers\*, Quinten Feys\*, Shoufeng Yang\*\*\*, Jef Vleugels \*\*, Jean-Pierre Kruth\*\*\*

\* KU Leuven, Department of Mechanical Engineering, division PMA, Celestijnenlaan 300, 3001 Heverlee, Belgium

\*\* KU Leuven, Department of Materials Engineering, Kasteelpark Arenberg 44, 3001 Heverlee, Belgium

\*\*\* KU Leuven, Department of Mechanical Engineering and member of Flanders Make, Virtual Department 3, Celestijnenlaan 300, 3001 Heverlee, Belgium

### Abstract

In this work, a slurry-based laser sintering process is investigated. Laser sintering allows for a broad palette of materials to be used. Since the binder content is only about 16 vol% with respect to the ceramic powder load, the debinding process is faster and less susceptible to crack formation and part warping compared to lithography-based manufacturing. The alumina slurry, used as a starting material for laser sintering, was optimized by adjusting the dispersant content to reach a minimum viscosity. After debinding and furnace sintering, multi-layer alumina parts with densities up to 97% were obtained.

Keywords: Alumina, Additive Manufacturing, Laser Sintering, Powder Metallurgy

### Introduction

Alumina ( $\text{Al}_2\text{O}_3$ ) ceramics cover about 40 % of the technical ceramic industry market. Applications can be found in the chemical industry (corrosion resistant material, filters), electronics (substrates), electrical engineering (spark plug insulators), high temperature environments (protective tubes for thermocouples, burner nozzles) and in the biomedical sector. Alumina ceramics are generally fabricated using a powder metallurgy process consisting of different steps. One of these steps is component shaping. Shaping can be done using a variety of techniques, depending on the desired geometry of the final component. For simple shapes, uniaxial or biaxial compaction is used, whereas more complex geometries can be obtained by injection moulding or slip casting. However, injection moulding is only economically justified for large series due to the high initial investment cost of the mould. Slip or pressure slip casting also requires a mould and is only viable for thin-walled geometries.

Additive manufacturing (AM) technologies can be complementary with conventional ceramic shaping techniques since they are suitable for the production of complex components in small series. Amongst the AM methods, lithography-based ceramic manufacturing (LCM) has already proven its viability for the production of small, intricate alumina parts [1] [2]. However, LCM has a limited materials palette, since some ceramics, like SiC, absorb the UV light and decrease the penetration depth and the degree of crosslinking in the polymer binder [3]. Additionally, the debinding process inherent to LCM is rather slow and time-consuming, in some cases taking multiple days [4].

Powder-bed fusion AM techniques, like laser sintering (LS), have the potential to overcome these drawbacks. For ceramic materials, laser sintering is usually done indirectly, meaning a sacrificial polymer binder is used [5]. A powder bed is deposited and scanned by a laser. The laser radiation is absorbed by the polymer binder and causes it to melt. The polymer binder resolidifies after the laser has passed, binding the ceramic particles together [6]. This process is repeated layer-by-layer until a 3D ‘green’ part, consisting of polymer and ceramic, is built. After debinding and sintering, the final ceramic part is obtained.

Laser sintering is conventionally performed on dry powder starting material. Various authors have attempted to produce dense alumina ceramics in this way, but reaching high densities proved difficult, as shown by Lakshminarayan et al. [7] [8], Shahzad [9] [10] and Deckers [11]. In order to improve the part density, slurry-based approaches can be considered. A slurry-based layer deposition leads to a higher powder packing density, reducing the amount of polymer binder required. The combination of a higher packing density and a lower amount of binder leads to higher green and final densities, as evidenced by Tang et al. [12], who produced alumina components using a slurry-based approach combined with laser sintering. Compared to the work of Shahzad and Deckers [9-11], the binder content is lower, resulting in higher final relative densities, as shown in Table 1.

Table 1: Dry powder-based (Deckers & Shahzad et al. [9-11]) compared to slurry-based approach (Tang et al. [12]).

	<b>Binder (vol%)</b>	<b>Rel. Density (%)</b>
Deckers & Shahzad et al. [9-11]	60	50-90
Tang et al. [12]	10-15	98

This paper presents a study on the use of slurry-based laser sintering as a shaping technique in a powder metallurgy process in order to produce freeform alumina parts with closed porosity, i.e. relative densities > 95%. The suggested powder metallurgy process is presented in Figure 1 and consists of 4 steps. Alumina is used as structural material (ceramic), whereas polyvinyl alcohol (PVA) is used as a sacrificial binder.

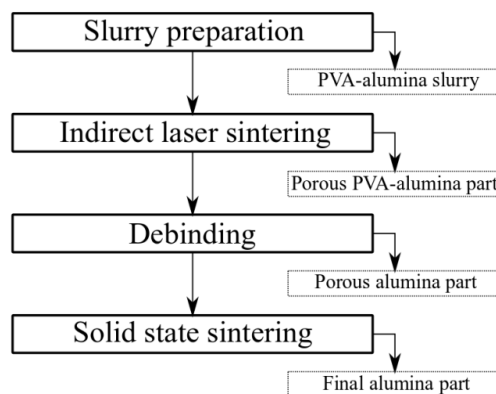


Figure 1: The powder metallurgy process used in this work, with indirect laser sintering as a shaping method to form complex alumina green parts.

## **Experimental Procedures**

### **Slurry Preparation**

The starting materials for slurry preparation are demineralised water, alumina powder ( $\text{Al}_2\text{O}_3$ , SM8, Baikowski, purity = 99.8%,  $d_{50} = 0.3 \mu\text{m}$ ) and polyvinyl alcohol (PVA, Sigma Aldrich, MW = 13.000-23.000). Dispex A40 (BASF), a solution of an ammonium salt of an acrylic polymer in water, was used as a dispersant. Finally, Contraspum K1012 (Zschimmer & Schwarz) was added as a defoamer to prevent air bubbles in the slurry.

The first step in the slurry preparation is the de-agglomeration of the alumina powder. For this purpose, 100 g of alumina powder was mixed in 25 ml of demineralised water and 0.1 to 2 g Dispex A40 in a polyethylene bottle. After adding 250 g of zirconia ( $\text{ZrO}_2$ , grade TZ-3Y, Tosoh) milling media (diameter 10 mm), the bottle was mixed on a Turbula multidirectional mixer for 24 h. Afterwards, 6 g of the PVA binder was dissolved in another 25 g of demi-water at  $95^\circ\text{C}$  and added to the de-agglomerated alumina mixture. The slurry was mixed for 30 min using a handheld mixing device. Finally, 1 ml of Contraspum was added and the slurry was lightly stirred until all of the air bubbles had disappeared.

### **Slurry Deposition**

The prepared slurry was kept in a polyethylene bottle, which was connected to a silicone tube. A peristaltic pump was used to supply the slurry through this silicone tube to a deposition nozzle that was attached to the coater system of a refurbished laser sintering machine. This deposition nozzle, shown in Figure 2, consists of many different channels and allows the slurry to be deposited evenly on the base plate. A schematic of the machine and the refurbished slurry deposition system is shown in Figure 3, while the actual set-up is presented in Figure 4.

Every time a layer is to be deposited, the pump supplies a certain amount of slurry on the build plate of the machine through the deposition nozzle, in front of the coater. The coater then moves over the build plate and spreads the deposited slurry evenly over the surface.



Figure 2: Deposition nozzle for an even slurry supply and deposition on the build plate of the laser sintering machine.

## Laser Sintering

Laser sintering was done on an in-house refurbished EOSINT M250 machine. The machine was equipped with a 60 W continuous wave CO<sub>2</sub> laser and a peristaltic pump for slurry deposition. The process chamber was filled with inert N<sub>2</sub> gas in order to prevent thermal oxidation of the PVA. A wide range of parameter sets was used to scan various batches of 10x10x5 mm<sup>3</sup> cubes in order to find the optimal window for laser sintering. Laser powers were ranged from 2 to 8 W and scanning speeds from 100-300 mm/s, while the layer thickness and hatch spacing were kept constant at 30 μm and 70 μm respectively. The build platform was preheated to a temperature of 50°C in order to facilitate layer drying. Scanning was done in a continuous zig-zag pattern, with a rotation of 90 degrees in between layers.

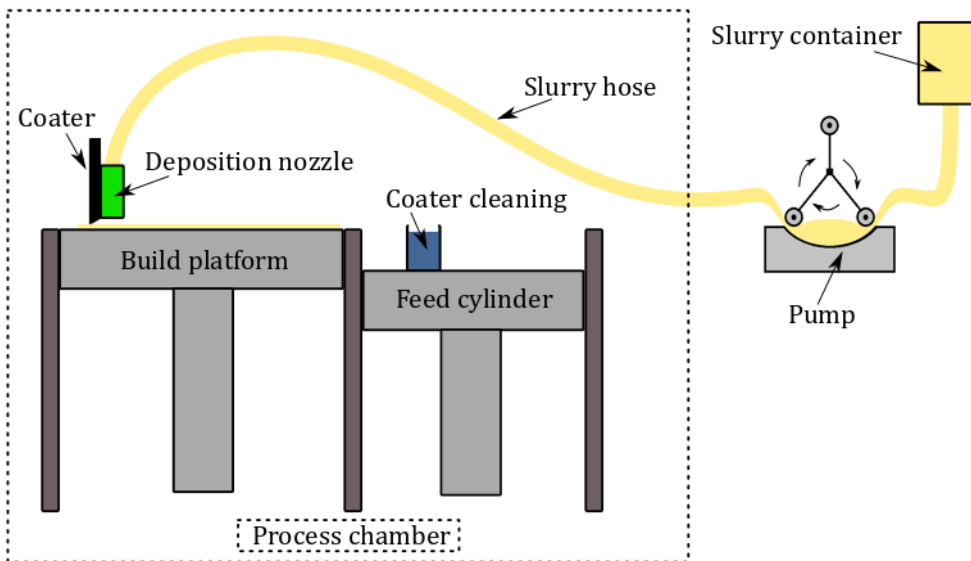


Figure 3: Schematic of the refurbished laser sintering machine for ceramic slurry-based laser sintering.

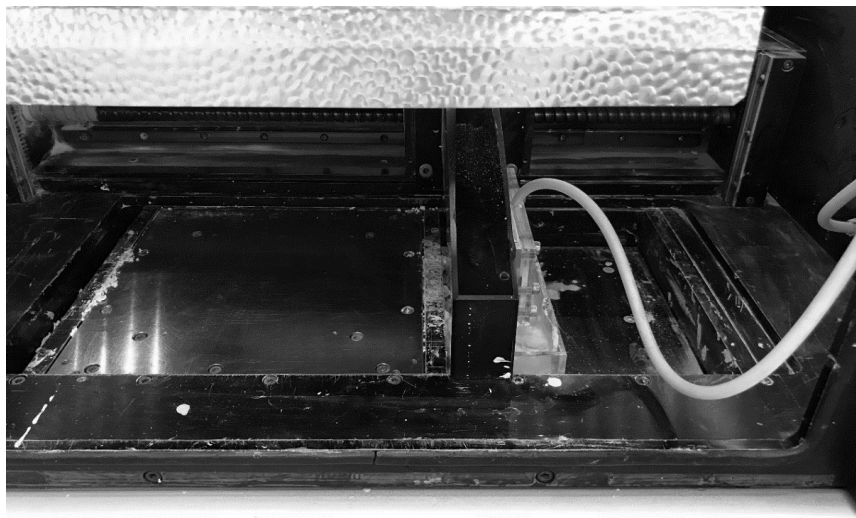


Figure 4: Process chamber of the refurbished laser sintering machine for ceramic slurry-based laser sintering, with build plate, coater, deposition nozzle, slurry tube and cleaning system.

### Debinding & Sintering

Debinding was done in a muffle furnace (Carbolite) operating under ambient conditions. The laser sintered green parts were placed in an alumina crucible and heated at  $1^{\circ}\text{C}/\text{min}$  to  $600^{\circ}\text{C}$  to allow the PVA polymer binder to oxidise. The holding time at  $600^{\circ}\text{C}$  was 1 hour, and the parts were subsequently cooled down naturally. The sample-containing crucible was then transferred to a high temperature chamber furnace (Nabertherm) for sintering. The heating rate for sintering was  $10^{\circ}\text{C}/\text{min}$  up to  $1100^{\circ}\text{C}$ , with a thermal homogenisation holding time of 1 h, and  $5^{\circ}\text{C}/\text{min}$  up to  $1600^{\circ}\text{C}$ , where they were held for another 2 h before naturally cooling by a furnace switch-off.

### Measurements

The viscosity of the alumina slurries was measured using a rheometer equipped with a cone-plate geometry (MCR501, Anton Paar GmbH, Austria) at a constant shear rate of  $1\text{ s}^{-1}$ . Density measurements were performed using the Archimedes method (Acculab atilon ATL-244-1), assuming a theoretical density of  $3.96\text{ g}/\text{cm}^3$  for  $\text{Al}_2\text{O}_3$ . Micrographs were taken using either optical microscopy (3D Digital Microscope Keyence VHX-6000) or scanning electron microscopy (SEM, FEI XL30-FEG) in order to study the microstructural features and defects in the sintered alumina objects.

### Results & Discussion

Viscosity testing was performed on 32 vol % alumina slurries with varying amounts of Dispex A40 in order to determine the optimal amount of dispersant. Dispex A40 was added to the slurry in different weight percentages with respect to alumina, ranging from 0 to 2 wt%. The resulting viscosities are presented in Figure 5.

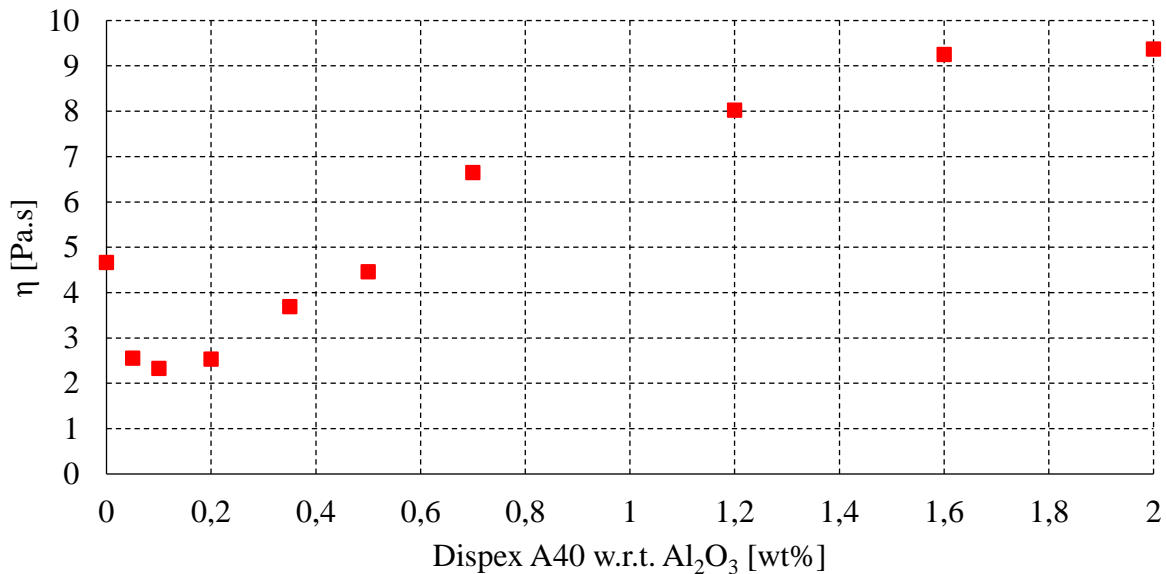


Figure 5: Viscosity of the 32 vol % alumina slurry as a function of the wt % dispersant.

A minimum can be observed at a Dispex A40 content of 0.1 wt%, relative to alumina. This can be explained by the working principle of the added dispersant. The carboxylic functional group of the Dispex A40 grafts to the alumina particle surface, whereas the polymer chain stretches out in the aqueous solvent effectively inhibiting the alumina particles to agglomerate by steric stabilisation. If the amount of dispersant is lower than the optimal value, the alumina particles are not completely coated with the polymer chains, causing some agglomeration and an increase in viscosity. However, when the amount of dispersant is higher than the optimal value, the alumina particles are completely coated and some residual polymer chains are present in the slurry. These thicken the fluid phase and can cause particle attraction through depletion forces. This, again, causes an increase in viscosity, as illustrated for Dispex concentrations above 0.2 wt% in Figure 5.

The optimized 32 vol % Al<sub>2</sub>O<sub>3</sub> slurry with 0.1 wt% of Dispex A40 was used for laser sintering. The composition of this slurry in volume percentages is summarized in Table 2. The packing density of the deposited and dried layers of this slurry were measured to be 60%, which is close to the theoretically achievable maximum value of 64% for randomly packed monomodal powder. A theoretical density of 3.54 g/cm<sup>3</sup> was used to calculate this, based on the volume fractions of ceramic versus polymer in the slurry.

Table 2: optimized slurry composition.

Water	PVA	Dispex A40	Al <sub>2</sub> O <sub>3</sub>	K1012
61.7 vol%	5.8 vol%	0.1 vol%	31.2 vol%	1.2 vol%

Laser sintering was done successfully with laser powers of 2-8 W and scanning speeds of 100-300 mm/s. After debinding and sintering, the density was measured using the Archimedes method. The density is plotted as a function of the laser energy density in Figure 6, which combines the most important laser sinter processing parameters and is a measure of how much laser energy is applied to the powder bed during laser sintering:

$$E = \frac{P}{v * l * s} \left( \frac{J}{mm^3} \right)$$

With:

- E in J/mm<sup>3</sup>, the laser energy density;
- P in W, the applied laser power;
- v in mm/s, the applied scanning speed;
- l in mm, the layer thickness and;
- s in mm, the hatch spacing.

As shown in Figure 6, the relative sintered densities hover between 95-97%, pointing to closed porosity. The relative density varies with the laser energy density, but there is no clear trend. This can be due to the nature of the porosity, which might not be influenced by the laser sintering itself, but caused by an uneven drying of the slurry layer during laser sintering, leading to inhomogeneous debinding and sintering and concomitant cracking in the final parts.

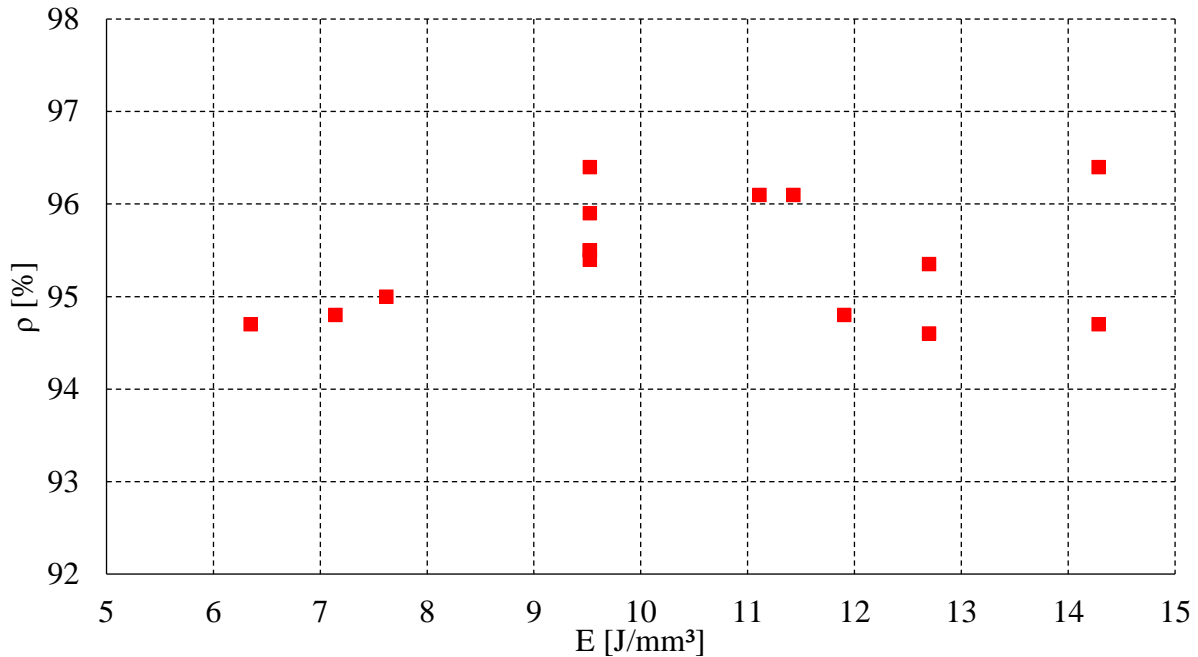


Figure 6: Relative density versus laser energy density for sintered alumina parts shaped by slurry-based laser sintering.

In order to investigate the nature of the porosity more closely, optical and SEM micrographs were taken. Optical micrographs of two parts scanned with a laser power of 3 and 4 W and scanning speeds of 100 and 200 mm/s respectively are presented in Figure 7 and Figure 8.

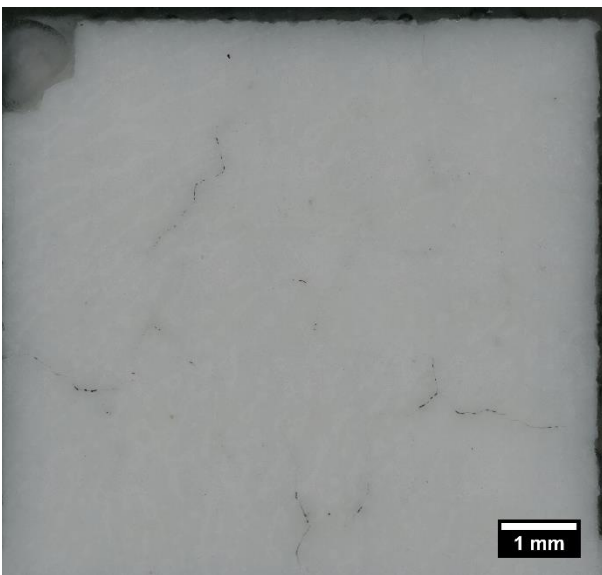


Figure 7: Stitched optical microscopy image of a sintered alumina part, laser sintered with a laser power of 3 W and a scanning speed of 100 mm/s ( $E = 14.3 \text{ J/mm}^3$ ,  $\rho = 96.4\%$ ). Top view.

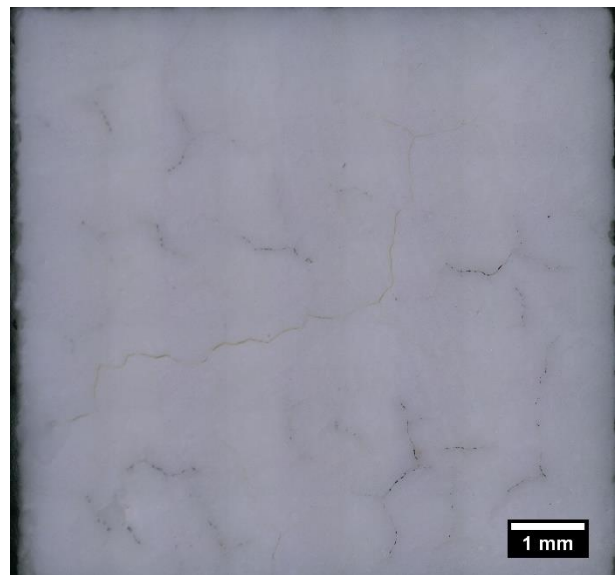


Figure 8: Stitched optical microscopy image of a sintered alumina part, laser sintered with a laser power of 4 W and a scanning speed of 200 mm/s ( $E = 9.5 \text{ J/mm}^3$ ,  $\rho = 95.9\%$ ). Top view.

Both micrographs show dense areas interrupted by cracks. The rather unusual patched crack pattern is most likely the result of an inhomogeneity in the slurry during drying. This is most probably caused by the fact that the slurry layers were not sufficiently dry when scanned by the laser. The laser then causes steam formation and/or water flow, which is accompanied with particle flow. This leads to alumina-rich and alumina-poor areas in the green part, which results in an inhomogeneous density and shrinkage cracks after solid-state sintering, as shown in Figure 7 and Figure 8.

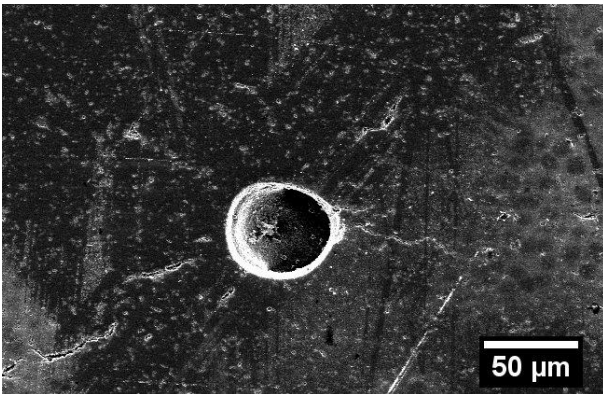


Figure 9: Close-up of a round pore and micro-cracks in an alumina part laser sintered with a power of 3 W and a scanning speed of 100 mm/s ( $E = 14.3 \text{ J/mm}^3$ ,  $\rho = 96.4\%$ ). Top view.

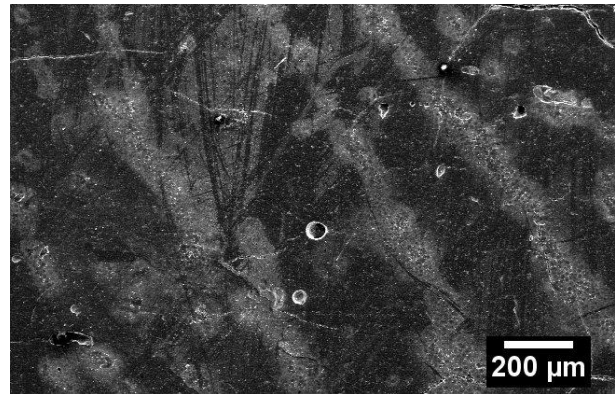


Figure 10: Crack pattern in an alumina part laser sintered with a power of 3 W and a scanning speed of 100 mm/s ( $E = 14.3 \text{ J/mm}^3$ ,  $\rho = 96.4\%$ ). Top view.

Cracks and round pores can also be observed on the SEM pictures in Figure 9 and Figure 10 of the material scanned with a laser power of 3 W and scanning speed of 100 mm/s (the same as the one in Figure 7). In order to overcome the cracking, two different options can be explored. Firstly, the water in the slurry layers can be removed by draining it through a porous substrate rather than evaporating it by pre-heating and laser scanning. Secondly, cold isostatic pressing could be performed after laser sintering. This might close the existing cracks and lead to a more homogeneous debinding and solid-state sintering.

### Summary

Slurry-based laser sintering was used as a shaping step to form alumina ceramics. The dispersant content of the slurry was optimized by means of viscosity testing. The optimized slurry was used in a refurbished laser sintering machine and green parts were fabricated. After debinding and solid-state sintering, closed porosity densities up to 97% were reached. Compared to dry powder-based approaches, where densities were in a range from 50% to 90% depending on the amount of post-processing techniques used, the slurry-based approach yields a clear improvement. This is largely due to the increased powder packing density and the decreased binder content of only 15 vol%, leading to denser green and final parts. However, cracks are still present, pointing to inhomogeneous sintering. This is likely caused by insufficiently dry slurry layers being scanned by the laser, resulting in steam formation and alumina particle re-arrangement. This leads to varying packing- and green densities throughout the scanned part and an inhomogeneous final density and shrinkage cracks.

## Acknowledgements

This work was financially supported by the Research Foundation – Flanders (FWO) under project FWO-G.0956.14N. The authors acknowledge support of the research fund of KU Leuven through Project GOA/15/012-SUMMA and wish to thank Dr. Sam Buls, Mr. Yannis Kinds, Mr. Louca R. Goossens, Mr. Stijn Schoeters and Mr. Carsten Bakker for the machine refurbishment.

## References

- [1] “Lithoz' LCM-Technology,” Lithoz, [Online]. Available: <http://www.lithoz.com/en/additive-manufacturing/lcm-technology>. [Accessed 17 May 2018].
- [2] “About the ADMAFLEX technology,” Admatec, [Online]. Available: <https://admateceurope.com/>. [Accessed 17 May 2018].
- [3] A. Badev, Y. Abouliatim, T. Chartier, L. Lecamp, P. Lebaudy, C. Chaput and C. Delage, “Photopolymerization kinetics of a polyether acrylate in the presence of ceramic fillers used in stereolithography,” *Journal of Photochemistry and Photobiology A: Chemistry*, vol. 222, no. 1, pp. 117-122, 2011.
- [4] U. Scheithauer, E. Schwarzer, E. Moritz and A. Michaelis, “Additive Manufacturing of Ceramic Heat Exchanger: Opportunities and Limits of the Lithography-Based Ceramic Manufacturing (LCM),” *Journal of Materials Engineering and Performance*, vol. 27, no. 1, pp. 14-20, 2018.
- [5] J. W. Barlow and N. K. Vail, "Producing high-temperature parts by low temperature sintering". International Patent WO 93/19019, 1993.
- [6] J.-P. Kruth, G. Levy, F. Klocke and T. Childs, “Consolidation phenomena in laser and powder-bed based layered manufacturing,” *CIRP Annals - Manufacturing Technology*, vol. 56, no. 2, pp. 730-759, 2007.
- [7] U. Lakshminarayan, S. Ogrzydiziak and H. L. Marcus, “Selective Laser Sintering of ceramic materials,” in *Proceedings of the Solid Freeform Fabrication Symposium*, Austin, Texas, 1990.
- [8] U. Lakshminarayan and H. L. Marcus, “Microstructural and mechanical properties of Al<sub>2</sub>O<sub>3</sub>/P<sub>2</sub>O<sub>3</sub> and Al<sub>2</sub>O<sub>3</sub>/B<sub>2</sub>O<sub>3</sub> composites fabricated by selective laser sintering,” in *Proceedings of the Solid Freeform Fabrication Symposium*, Austin, Texas, 1991.
- [9] K. Shahzad, J. Deckers, S. Boury, B. Neirinck, J.-P. Kruth and J. Vleugels, “Preparation and indirect selective laser sintering of alumina/PA microspheres,” *Ceramics International*, vol. 38, pp. 1241-1247, 2012.
- [10] K. Shahzad, J. Deckers, J.-P. Kruth and J. Vleugels, “Additive manufacturing of alumina parts by indirect selective laser sintering and post processing,” *Journal of Materials Processing Technology*, vol. 213, pp. 1484-1494, 2012.
- [11] J. Deckers, K. Shahzad, J. Vleugels and J.-P. Kruth, “Isostatic pressing assisted indirect selective laser sintering of alumina components,” *Rapid Prototyping Journal*, vol. 18, pp. 409-419, 2012.

- [12] H.-H. Tang, M.-L. Chiu and H.-C. Yen, "Slurry-based selective laser sintering of polymer-coated ceramic powders to fabricate high strength alumina parts," *Journal of the European Ceramic Society*, vol. 31, pp. 1383-388, 2011.